Chemical Science

ROYAL SOCIETY OF CHEMISTRY

EDGE ARTICLE

View Article Online
View Journal | View Issue

Cite this: *Chem. Sci.*, 2020, **11**, 8000

All publication charges for this article have been paid for by the Royal Society of Chemistry

Received 19th April 2020
Accepted 2nd July 2020

DOI: 10.1039/d0sc02207a

rsc.li/chemical-science

The precise editing of surface sites on a molecular-like gold catalyst for modulating regioselectivity†

Shuohao Li,‡ Hongwei Chen,‡ Xu Liu, Haoqi Liu, Jing Ma * and Yan Zhu *

It is extremely difficult to precisely edit a surface site on a typical nanoparticle catalyst without changing other parts of the catalyst. This precludes a full understanding of which site primarily determines the catalytic properties. Here, we couple experimental data collection with theoretical analysis to correlate rich structural information relating to atomically precise gold clusters with the catalytic performance for the click reaction of phenylacetylene and benzyl azide. We also identify a specific surface site that is capable of achieving high regioselectivity. We further conduct site-specific editing on a thiolate-protected gold cluster by peeling off two monomeric RS–Au–SR motifs and replacing them with two $Ph_2P–CH_2–PPh_2$ staples. We demonstrate that the surface Au–$Ph_2P–CH_2–PPh_2$–Au motifs enable extraordinary regioselectivity for the click reaction of alkyne and azide. The editing strategy for the surface motifs allows us to exploit previously inaccessible individual active sites and elucidate which site can explicitly govern the reaction outcome.

Introduction

The identification of catalytically active sites in particle catalysts has long been an important task in catalytic chemistry.[1–3] In the sub-nanometer size regime, each site of a catalyst may be directly or indirectly involved in a reaction process.[4–6] Hence, it is highly desirable to explicitly conclude the extents to which individual sites of a catalyst contribute to its overall catalytic performance. However, due to the complexity of conventional investigations, it remains an open challenge to directly observe the catalytic performance of each site in a typical catalyst; microscopy and spectroscopy techniques usually provide statistically averaged or sample-averaged information.[7] Enlightened by organic chemists who can deliberately remove or replace any group in an organic molecule without changing other parts, tailoring a specific site without changing the other parts of a solid catalyst would allow us to unveil the contribution of the specific site to a given chemical reaction.

Atomically precise metal clusters constitute a new generation of metal catalysts in catalysis science and exhibit unexpected catalytic properties.[8–13] These metal clusters provide the potential to precisely correlate intricate structural information (such as aesthetic structural pattern, ligand effect, metal–metal bonding, metal–ligand interfacial bonding, and metal charge) with the catalytic properties, which can shed light on current mysteries in the field of catalysis.[14–21] By solving their atomic structures, we can determine the active site structure and establish definitive structure–property relationships, which have previously been elusive.[22] Such advances in these clusters inspire us to use them as proof-of-concept catalysts to pursue a fundamental understanding of how a specific site in a catalyst controls the catalytic properties.

In this work, the cycloaddition reaction of alkyne and azide by means of click chemistry, which has been widely applied to generate high-value organic compounds, was chosen as a probe reaction.[23] A series of ligand-protected Au_n (n = gold atom number) clusters with different atomic structures and surface motifs (see ESI for structural details, Fig. S1†) were screened to catalyze the click reaction. As shown in Fig. 1, these Au_n clusters failed to provide regioselectivity for the 1,4- or 1,5-triazole products of the click reaction of phenylacetylene and benzyl azide. The above Au_n clusters could not selectively drive the reaction process toward either of the two products. We thus questioned whether a purposeful editing on the surface motifs of the clusters might be used to manipulate the regioselectivity toward one product. If successful, this promising strategy could be developed to precisely modulate the surface active sites of catalysts to obtain an exclusive product through an operative process.

Results and discussion

Given the complexity of the geometric structures and surface structures of the Au_n clusters, it is difficult to rapidly identify the key structures in inducing high regioselectivity toward an exclusive product. Therefore, we analyzed the relationships

School of Chemistry and Chemical Engineering, Nanjing University, Nanjing 210093, China. E-mail: zhuyan@nju.edu.cn; majing@nju.edu.cn

† Electronic supplementary information (ESI) available. See DOI: 10.1039/d0sc02207a

‡ These authors contributed equally to this work.

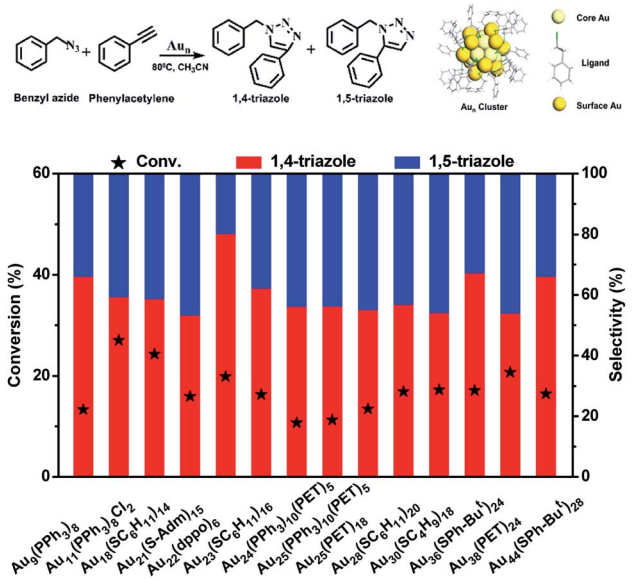

Fig. 1 The catalytic performances of ligand-protected Au_n catalysts for the click reaction of phenylacetylene and benzyl azide. Reaction conditions: 2 mg of Au_n, phenylacetylene (0.15 mmol), benzyl azide (0.15 mmol), 2 ml of acetonitrile, 80 °C, 5 h. The upper panel shows the scheme for the click reaction of phenylacetylene and benzyl azide and a general model of Au_n clusters. PET = 2-phenylethanethiol; S-Adm = 1-adamantanethiolate; dppo = 1,8-bis(diphenyl-phosphino)octane.

between the structural information of the Au_n clusters with the reaction activity and selectivity using existing reaction data (Fig. 1) to aid in establishing the structure–property relationship. Fig. 2a shows the effect of the surface gold atoms on the catalytic activity. In general, more surface gold atoms resulted in higher catalytic activity (more details of surface Au atoms are shown in Fig. S2†). It is interesting to consider the steric hindrance effect of the ligands on the regioselectivity of these Au_n clusters protected by thiolates (Fig. 2b). Steric hindrance was qualitatively expressed by the surface area occupied by each ligand (*i.e.*, the ratio of the total van der Waals surface area to the number of ligands of a cluster, referred to as the surface area per ligand). The steric hindrance effect of the ligands can also be illustrated by the electrostatic potentials of the Au_n clusters determined by density functional theory (DFT) calculations,[24] as shown in Fig. 2b and c (more details can be found in Fig. S3 and Table S1†). On the other hand, in the systems of the Au_n clusters capped by PPh_3 ligands, the steric hindrance is larger than in the thiolate-protected clusters. The Au_n clusters capped by PPh_3 ligands show larger surface areas per ligand and much narrower pockets for reactant docking (compared Fig. 2b and c). More interestingly, the steric hindrance from PPh_3 ligands is strongly correlated to the regioselectivity of the 1,4-product (Fig. 2c). Thus, the results suggest that the Au_n clusters capped by phosphine ligands relative to thiolates are prone to driving the click reaction pathway toward the 1,4-product compared to Au_n clusters capped by thiolates.

Inspired by the workable molecular tailoring of the $Au_{23}(SR)_{16}$ cluster,[25] the specific surface site containing phosphine ligands (Au–Ph_2P–CH_2–PPh_2–Au) was selected to enable

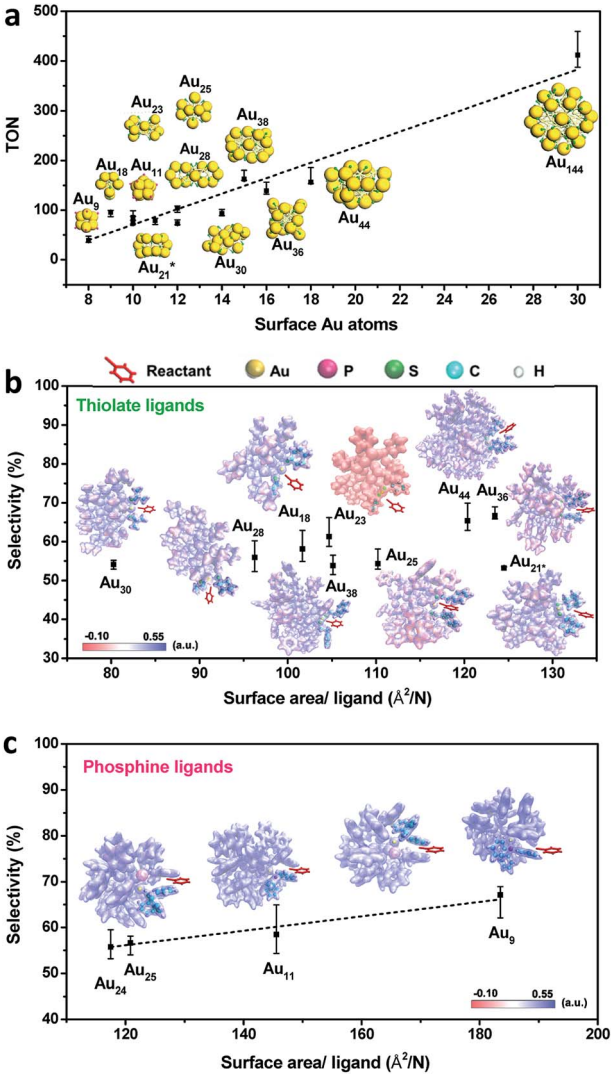

Fig. 2 (a) Correlation between the catalytic activity and the surface Au atoms of Au_n clusters. The insets show the atomic structures of the clusters. Color codes: yellow = Au; green = S; pink = P. (b) The relationship between the catalytic selectivity for 1,4-triazole and steric hindrance in thiolate-protected Au_n clusters. $Au_{21*} = Au_{21}(S\text{-}Adm)_{15}$. (c) The relationship between the catalytic selectivity for 1,4-triazole and the steric hindrance in PPh_3-protected Au_n clusters. The insets in (b) and (c) illustrate the electrostatic potentials of Au_n clusters from DFT calculations.

regioselectivity in the click reaction. As illustrated in Fig. 3a, the $Au_{23}(SR)_{16}$ cluster possesses an Au_{13} cuboctahedron protected by two trimeric $Au_3(SR)_4$ staple motifs, two monomeric RS–Au–SR staples, and four bridging SR thiol ligands.[26] By the resection of two monomeric RS–Au–SR motifs of the $Au_{23}(SR)_{16}$ cluster (abbreviated as Au_{23}) and bandaging the gaps with two Ph_2P–CH_2–PPh_2 staples, the $Au_{21}(SR)_{12}(Ph_2PCH_2PPh_2)_2$ cluster (abbreviated as Au_{21}) was obtained (Fig. 3a). The two clusters showed similar UV-vis optical spectra (Fig. S4†) and hold similar atomic structures, with the exception that RS–Au–SR is replaced by Ph_2P–CH_2–PPh_2. As shown in Fig. 3b, the peak corresponding to the mass/charge ratio (m/z) of 6371.09 was observed in the electrospray ionization mass spectrum (ESI-MS), corresponding

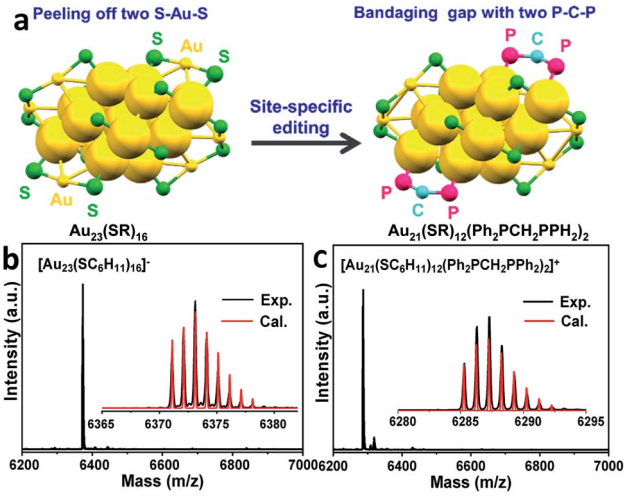

Fig. 3 (a) A schematic diagram of the site-specific editing of $Au_{23}(SR)_{16}$ by resecting two RS–Au–SR motifs and bandaging the gaps with two $Ph_2P–CH_2–PPh_2$ staples to obtain $Au_{21}(SR)_{12}(Ph_2PCH_2PPh_2)_2$. Color codes: yellow = Au; green = S; pink = P; blue = C. Carbon tails are omitted for clarity. SR = cyclohexanethiol. The ESI-MS spectra of (b) $[Au_{23}(SC_6H_{11})_{16}]^-$ and (c) $[Au_{21}(SC_6H_{11})_{12}(Ph_2PCH_2PPh_2)_2]^+$.

to $[Au_{23}(SC_6H_{11})_{16}]^-$. The peak at m/z = 6285.3 in Fig. 3c was assigned to $[Au_{21}(SC_6H_{11})_{12}(Ph_2PCH_2PPh_2)_2]^+$.

As shown in Fig. 4a, $Au_{21}(SC_6H_{11})_{12}(Ph_2PCH_2PPh_2)_2$ exhibited a high selectivity for 1,4-triazoles. In contrast, the $Au_{23}(SC_6H_{11})_{16}$ cluster showed no regioselectivity for 1,4- or 1,5-triazoles under identical reaction conditions. The replacement of two surface RS–Au–SR motifs by two $Ph_2P–CH_2–PPh_2$ motifs successfully tuned the reaction pathway of the click reaction, leading to the transformation from non-regioselectivity to regioselectivity accompanied by the transformation from $Au_{23}(SC_6H_{11})_{16}$ to $Au_{21}(SC_6H_{11})_{12}(Ph_2PCH_2PPh_2)_2$. Additionally, $Au_{21}(SC_6H_{11})_{12}(Ph_2PCH_2PPh_2)_2$ exhibited better activity than $Au_{23}(SC_6H_{11})_{16}$ (Fig. 4a), which may be attributed to the stronger chemical adsorption capability of the former catalyst, as deduced from *in situ* time-resolved infrared Fourier transform infrared (FTIR) spectroscopic analysis of CO molecules adsorbed onto the two catalysts (Fig. S5†). The two clusters seemed robust during the reactions (Fig. S6 and S7†). Furthermore, the relationship between regioselectivity and steric hindrance in the $Au_{21}(SC_6H_{11})_{12}(Ph_2PCH_2PPh_2)_2$ and $Au_{23}(SC_6H_{11})_{16}$ systems was corroborated by the analysis of the surface area/ligand ratio. The steric hindrance from the organic ligands can be significantly increased by the site-specific replacement of SR–Au–SR with $Ph_2P–CH_2–PPh_2$ (Fig. 4b), favoring an increase in regioselectivity toward 1,4-products.

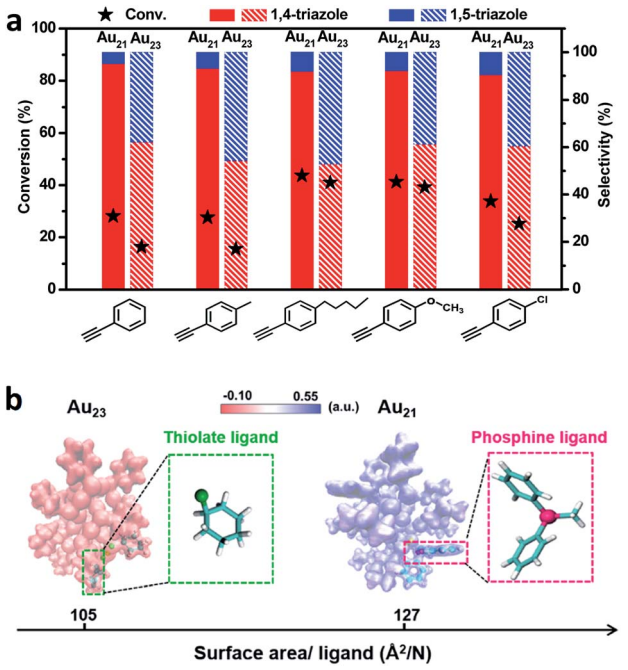

Fig. 4 (a) The catalytic performances of $Au_{21}(SC_6H_{11})_{12}(Ph_2PCH_2PPh_2)_2$ and $Au_{23}(SC_6H_{11})_{16}$ for the click reactions of alkynes and benzyl azide. The catalytic data are averaged over three independent measurements. (b) Steric hindrance from the surface ligands in the $Au_{21}(SC_6H_{11})_{12}(Ph_2PCH_2PPh_2)_2$ and $Au_{23}(SC_6H_{11})_{16}$ clusters. Color codes: yellow = Au; pink = P; green = S.

We now rationalize how $Au_{21}(SC_6H_{11})_{12}(Ph_2PCH_2PPh_2)_2$ can achieve regioselectivity while $Au_{23}(SC_6H_{11})_{16}$ cannot. First, the distinct selectivity cannot be attributed to the electronic structures of the two clusters because the exchange of surface motifs had little influence on the electronic properties of the clusters. As presented in Fig. 5a, the binding energies of the Au 4f X-ray photoelectron spectroscopy (XPS) peaks of $Au_{21}(SC_6H_{11})_{12}(Ph_2PCH_2PPh_2)_2$ were not noticeably difference from those of $Au_{23}(SC_6H_{11})_{16}$. The gold charge states were also monitored by X-ray absorption near-edge structure (XANES) studies, indicating that the gold charge state of Au_{21} was similar to that of Au_{23} based on liner combination fits (Fig. 5b and S8†). This means that tailoring the specific motifs did not cause a significant perturbation in the electronic structures of the two gold clusters.

Going further, the Au-acetylide intermediates on the $Au_{21}(SC_6H_{11})_{12}(Ph_2PCH_2PPh_2)_2$ and $Au_{23}(SC_6H_{11})_{16}$ clusters were studied by ^1H nuclear magnetic resonance (NMR) spectroscopy. Free phenylacetylene showed a singlet proton peak (δ = 3.1 ppm) and two sets of peaks (δ = 7.3 and 7.5 ppm) for the aromatic hydrogen atoms (Fig. 5c).[27] Of note, the acetylenic proton peak of phenylacetylene adsorbed on the $Au_{21}(SC_6H_{11})_{12}(Ph_2PCH_2PPh_2)_2$ cluster was nearly absent, excluding the

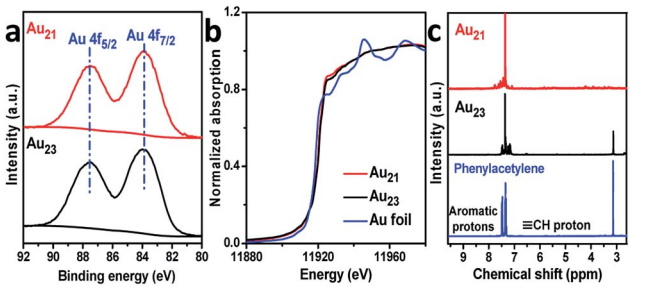

Fig. 5 (a) Au 4f XPS and (b) Au L_3-edge XANES profiles of $Au_{21}(SR)_{12}(Ph_2PCH_2PPh_2)_2$ and $Au_{23}(SR)_{16}$. (c) The ^1H NMR spectra of Au-acetylide species.

binding mode of phenylacetylene in the intact form (C≡C–H) and supporting its binding mode in the dehydrogenated form (C≡C) (Fig. S9†). In the $Au_{23}(SC_6H_{11})_{16}$ system, the peak of the ≡C–H proton is observed (Fig. 5c), although the peak intensity is weak, implying that the deprotonation-induced activation process of phenylacetylene was more difficult for $Au_{23}(SC_6H_{11})_{16}$ than for $Au_{21}(SC_6H_{11})_{12}(Ph_2PCH_2PPh_2)_2$. Taken together, the results imply that two binding modes of alkyne on $Au_{23}(SC_6H_{11})_{16}$ were obtained: terminal binding and internal binding (Fig. S9†).

To further understand the distinct catalytic regioselectivity of the $Au_{21}(SC_6H_{11})_{12}(Ph_2PCH_2PPh_2)_2$ and $Au_{23}(SC_6H_{11})_{16}$ clusters for the click reaction of phenylacetylene and benzyl azide, we performed DFT calculations to explore the possible reaction pathways of 1,4- and 1,5-product formation on the two clusters. The overall pathways may include the adsorption, coupling, and reductive elimination of azide and phenylacetylene. Fig. 6 shows the calculated energy profiles for the possible reaction pathways of phenylacetylene and benzyl azide in the $Au_{21}(SC_6H_{11})_{12}(Ph_2PCH_2PPh_2)_2$ model (the all-atom model, abbreviated as A-Au_{21}) and the $Au_{23}(SC_6H_{11})_{16}$ model (A-Au_{23}) along with the calculated reaction barriers. For the A-Au_{21} catalyst (Fig. 6 and S10†), the energy difference between the activation barrier for the pathway toward the 1,4-product ($\Delta G_{1,4}$ = 12.2 kcal mol^{-1}) and that for the pathway toward the 1,5-product ($\Delta G_{1,5}$ = 30.0 kcal mol^{-1}) was large ($\Delta\Delta G$ = 17.8 kcal mol^{-1}). Thus, the formation of 1,4-triazole on the Au_{21} catalyst is kinetically favored, resulting in regioselectivity on Au_{21}. The larger the energy difference $\Delta\Delta G$, the greater the selectivity for the 1,4-triazole. The large energy difference is related to the oxidative coupling of phenylacetylene and benzyl azide, which results in the generation of the six-membered intermediate IN1 (Fig. S11†). For A-Au_{21}-$IN1_{1,4}$, the carbon atom on phenylacetylene is firmly bound by two gold atoms, resulting in a more stable intermediate, while the carbon atom is only captured by one gold atom in the intermediate A-Au_{21}-$IN1_{1,5}$ (Fig. S11†). The click reaction occurs preferably on the Au–Au_P–P–P–Au_P–Au (Au_P denotes the Au atom attached to the phosphine ligand) and Au–S–Au sites of the Au_{21} catalyst. In contrast, for the A-Au_{23} catalyst (Fig. 6 and S10†), the energy difference between the 1,4-product and 1,5-product is relatively small ($\Delta\Delta G$ = 8.6 kcal mol^{-1}), leading to comparable selectivity for the formation of the 1,4- and 1,5-triazoles. This rationalizes the non-regioselectivity of the Au_{23} cluster. Similar trends were observed for simplified models of Au_{21} and Au_{23} (S-Au_{21} and S-Au_{23}; Fig. S12 and S13†), for which the energy differences between the pathways toward the 1,4-product and the 1,5-product over the S-Au_{21} and S-Au_{23} catalysts were 19.2 and 3.1 kcal mol^{-1} (Fig. S14†), respectively, in good agreement with the experimental results.

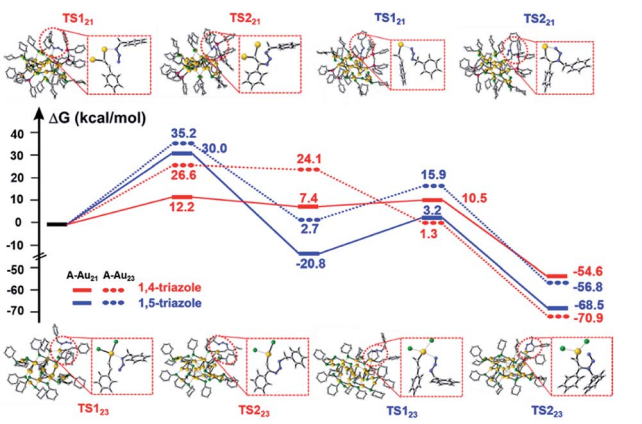

Fig. 6 DFT-calculated energy profiles for the reaction pathways of Au_{21} and Au_{23} clusters with the all-atom models, termed A-Au_{21} and A-Au_{23}. The insets indicate the reactive sites in the transition states. Color codes: yellow = Au, green = S, pink = P, gray = C, blue = N. To improve clarity, all the hydrogen atoms are hidden. TS = transition state.

Conclusions

In summary, we have demonstrated that site-specific editing on an $Au_{23}(SC_6H_{11})_{16}$ cluster *via* the exchange of the surface RS–Au–SR motifs with Ph_2P–CH_2–PPh_2 staples can achieve a transformation from non-regioselectivity to regioselectivity for the click reaction of azide and alkyne. The editing strategy for surface motifs offers an exciting opportunity to elucidate how a surface site of a catalyst can precisely control the reaction pathway. This work not only improves the understanding of the contribution of a single site in a solid catalyst to the overall catalytic performance, but it can also guide the development of a feasible strategy to enable highly efficient chemical processes based on the editing of surface sites of catalysts with atomic precision.

Conflicts of interest

There are no conflicts to declare.

Acknowledgements

We acknowledge financial support from the National Natural Science Foundation of China (21773109, 91845104, 21673111, 21873045).

Notes and references

1 M. Chen and D. W. Goodman, *Chem. Soc. Rev.*, 2008, **37**, 1860–1870.
2 S. Kattel, P. J. Ramírez, J. G. Chen, J. A. Rodriguez and P. Liu, *Science*, 2017, **355**, 1296–1299.
3 H. T. Chung, D. A. Cullen, D. Higgins, B. T. Sneed, E. F. Holby, K. L. More and P. Zeleny, *Science*, 2017, **357**, 479–484.
4 S. Xie, H. Tsunoyama, W. Kurashige, Y. Negishi and T. Tsukuda, *ACS Catal.*, 2012, **2**, 1519–1523.
5 K. Kwak, W. Choi, Q. Tang, M. Kim, Y. Lee, D. Jiang and D. Lee, *Nat. Commun.*, 2017, **8**, 14723.
6 Y. Liu, X. Chai, X. Cai, M. Chen, R. Jin, W. Ding and Y. Zhu, *Angew. Chem., Int. Ed.*, 2018, **57**, 9775–9779.

7 Y. Zhang, P. Song, T. Chen, X. Liu, T. Chen, Z. Wu, Y. Wang, J. Xie and W. Xu, *Proc. Natl. Acad. Sci. U. S. A.*, 2018, **115**, 10588–10593.
8 M. Turner, V. B. Golovko, O. P. H. Vaughan, P. Abdulkin, A. Berenguer-Murcia, M. S. Tikhov, B. F. G. Johnson and R. M. Lambert, *Nature*, 2008, **454**, 981–983.
9 E. C. Tyo and S. Vajda, *Nat. Nanotechnol.*, 2015, **10**, 577–588.
10 X. Wan, J. Wang, Z. Nan and Q. Wang, *Sci. Adv.*, 2017, **3**, e1701823.
11 Y. Tan, X. Liu, L. Zhang, A. Wang, L. Li, X. Pan, S. Miao, M. Haruta, H. Wei, H. Wang, F. Wang, X. Wang and T. Zhang, *Angew. Chem., Int. Ed.*, 2017, **56**, 2709–2713.
12 H. Chen, C. Liu, M. Wang, C. Zhang, N. Luo, Y. Wang, H. Abroshan, G. Li and F. Wang, *ACS Catal.*, 2017, **7**, 3632–3638.
13 H. Zhang, H. Liu, Z. Tian, D. Lu, Y. Yu, S. Cestellos-Blanco, K. K. Sakimoto and P. Yang, *Nat. Nanotechnol.*, 2018, **13**, 900–905.
14 Y. Wang, X. Wan, L. Ren, H. Su, G. Li, S. Malola, S. Lin, Z. Tang, H. Häkkinen, B. K. Teo, Q. Wang and N. Zheng, *J. Am. Chem. Soc.*, 2016, **138**, 3278–3281.
15 Y. Zhu, H. Qian and R. Jin, *J. Mater. Chem.*, 2011, **21**, 6793–6799.
16 T. Imaoka, H. Kitazawa, W. Chun, S. Omura, K. Albrecht and K. Yamamoto, *J. Am. Chem. Soc.*, 2013, **135**, 13089–13095.
17 W. Chen and S. Chen, *Angew. Chem., Int. Ed.*, 2009, **48**, 4386–4389.
18 C. Liu, X. Ren, F. Lin, X. Fu, X. Lin, T. Li, K. Sun and J. Huang, *Angew. Chem., Int. Ed.*, 2019, **58**, 11335–11339.
19 Q. Zhang, X. Chen and L. Wang, *Acc. Chem. Res.*, 2018, **51**, 2159–2168.
20 T. Imaoka, S. Tsuchiya and K. Yamamoto, *Chem. Lett.*, 2016, **45**, 1450–1452.
21 Y. Zhang, P. Song, T. Chen, X. Liu, T. Chen, Z. Wu, Y. Wang, J. Xie and W. Xu, *Proc. Natl. Acad. Sci. U. S. A.*, 2018, **115**, 10588–10593.
22 R. Jin, C. Zeng, M. Zhou and Y. Chen, *Chem. Rev.*, 2016, **116**, 10346–10413.
23 J. E. Moses and A. D. Moorhouse, *Chem. Soc. Rev.*, 2007, **36**, 1249–1262.
24 W. Wang, X. Sun, J. Qu, X. Xie, Z. Qi, D. Hong, S. Jing, D. Zheng, Y. Tian, H. Ma, S. Yu and J. Ma, *Phys. Chem. Chem. Phys.*, 2017, **19**, 31443–31451.
25 Q. Li, J. C. Russell, T. Luo, X. Roy, N. L. Rosi, Y. Zhu and R. Jin, *Nat. Commun.*, 2018, **9**, 3871.
26 Q. Li, T. Luo, M. G. Taylor, S. Wand, X. Zhu, Y. Song, G. Mpourmpakis, N. L. Rosi and R. Jin, *Sci. Adv.*, 2017, **3**, e1603193.
27 W. Chen, J. R. Davies, D. Ghosh, M. Tong, J. P. Konopelski and S. Chen, *Chem. Mater.*, 2006, **18**, 5253–5259.